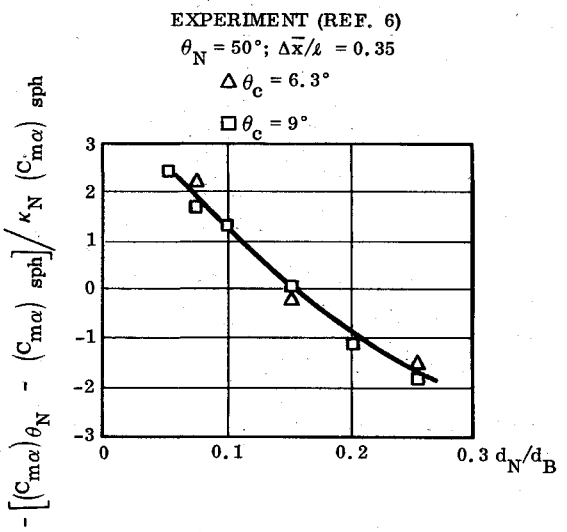

Fig. 5 Universal scaling of nose-tip directing ($C_{DN\alpha}$) effects for $\theta_N = 50°$.

emphasized that Fig. 4 can be defined using available data for spherically blunted cones. When the nose tip angle is not $\theta_N = 45°$ one has to determine the factor by which the nose-drag-induced loads obtained from Fig. 4 should be multiplied to give the complete loading on the frustum aft of a conical nose tip. Multiplying by the sharp cone values and adding the effect of nose tip lift (using modified Newtonian Theory, $C_{p\max} \approx 1.8$) would then give the sought prediction of experimental nonlinear characteristics. It should be emphasized that this whole procedure is valid only if the c.g. location in percent of sharp cone length remains the same.

Using Eq. (3) we find that the 6.3° cone at $\alpha = 3°$ would correspond to a 9° tangent cone at $\alpha = 0$, which in Fig. 4b places $d_N/d_B = 0.15$ right where the steep increase of dynamic stability will occur if the "effective cone angle" is increased further through increased angle of attack. This explains the steep increase of dynamic stability for $\alpha > 3°$ in Fig. 3.

References

[1] Walchner, O. and Clay, J., "Nose Bluntness Effects on the Stability Derivatives of Cones in Hypersonic Flow," *Transactions of the Second Technical Workshop on Dynamic Stability Testing*, Vol. 1, Paper 8, April 1965, Arnold Engineering Development Center, Arnold Air Force Station, Tullahoma, Tenn.

[2] Ward, L. K. Jr. and Uselton, B. L., "Dynamic Stability Results for Sharp and Blunt 10-Deg. Cones at Hypersonic Speeds," *Transactions of the 3rd Technical Workshop on Dynamic Stability Problems*, Vol. III, Paper 2, Nov. 1968, NASA Ames Research Center, Moffett Field, Calif.

[3] Malcolm, G. N. and Rakich, J. V., "Comparison of Free-Flight Experimental Results and Theory, on the Nonlinear Aerodynamic Effects of Bluntness for Slender Cones," *AIAA Journal*, Vol. 9, No. 3, March 1971, pp. 473–478.

[4] Rie, H., Linkievicz, E. A., and Bosworth, F. D., "Hypersonic Dynamic Stability, Part III, Unsteady Flow Field Program," FDL-TDR-64-149, Part III, Jan. 1967, Air Force Flight Dynamics Lab., Wright-Patterson Air Force Base, Chio.

[5] Ericsson, L. E., "Effect of Nose Bluntness, Angle of Attack, and Oscillation Amplitude on Hypersonic Unsteady Aerodynamics of Slender Cones," *AIAA Journal*, Vol. 9, No. 2, Feb. 1971, pp. 297–304.

[6] Neff, R. S., "Conical Nose Shape Effects on Drag and Stability at Mach 10," *Journal of Spacecraft and Rockets*, Vol. 9, No. 1, Feb. 1972, pp. 126–128.

[7] Ericsson, L. E. and Guenther, R. A., "Effect on Slender Vehicle Dynamics of Change from Spherical to Conical Nose Bluntness," *Journal of Spacecraft and Rockets*, Vol. 9, No. 6, June 1972, pp. 435–440.

[8] Ericsson, L. E., "Universal Scaling Laws for Hypersonic Nose Bluntness Effects," *AIAA Journal*, Vol. 7, No. 12, Dec. 1969 pp. 2222–2227.

Effect of Polarization on the Apparent Emittance of Rectangular Groove Cavities

C. L. TIEN*
University of California, Berkeley, Calif.

SEVERAL recent studies showed that the effect of polarization may become appreciable for radiant heat transfer among surfaces as a result of multiple reflections.[1-3] This effect is commonly neglected in evaluating the apparent emittance of surface cavities.[4,5] The present Note is to demonstrate the effect of polarization on the apparent emittance of rectangular groove cavities with specularly reflecting walls. It is also interesting to point out here that the present result is obtained directly from existing numerical results for long passage transmittance[2] through simple consideration.

Figure 1 shows a rectangular groove cavity with specularly reflecting walls. For convenience, consider $T_c > T_w$ and the radiant energy flux into the cavity is thus given by

$$q = \sigma(T_c^4 - T_w^4)\tau_{12} + \sigma(T_c^4 - T_w^4)\tau_{13} \tag{1}$$

where τ_{ij} is the transmittance between surfaces i and j. In accordance with the general definition of apparent emittance (or absorptance)[5]

$$\varepsilon = q/\sigma(T_c^4 - T_w^4) \tag{2}$$

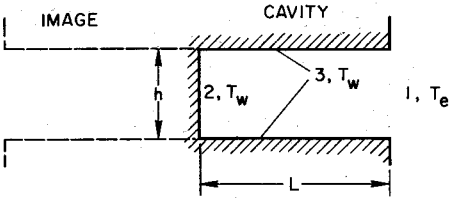

Fig. 1 Rectangular groove cavity.

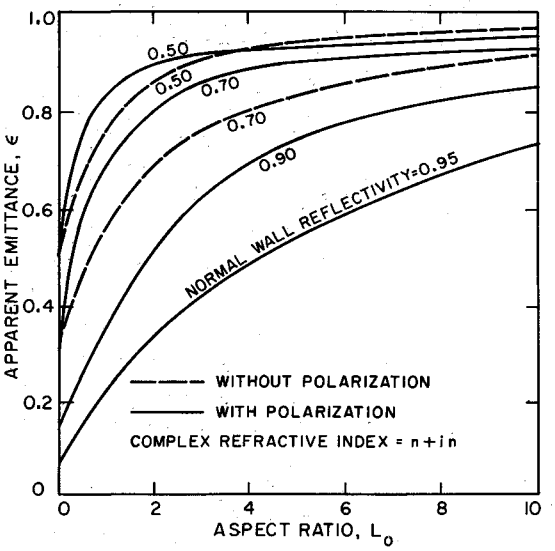

Fig. 2 Apparent emittance of rectangular groove cavities with specularly reflecting metallic walls.

Received February 18, 1972.
Index categories: Radiation and Radiative Heat Transfer; Thermal Surface Properties.

* Professor of Mechanical Engineering. Associate Fellow AIAA.

there results from Eq. (1)

$$\varepsilon = \tau_{12} + \tau_{13} \tag{3}$$

Through the consideration of energy balance and mirror image (Fig. 1), it can be established that

$$\tau_{12} = \tau(L_0) - \rho\tau(2L_0) \tag{4}$$

and

$$\tau_{13} = 1 - (1-\rho)\tau(L_0) - \rho\tau(2L_0) \tag{5}$$

where L_0 (aspect ratio) $= L/h$ and ρ is the hemispherical specular reflectance of cavity walls. Thus, the apparent emittance can be simply expressed as

$$\varepsilon = 1 - \rho[2\tau(2L_0) - \tau(L_0)] \tag{6}$$

and evaluated by substituting the numerical values of transmittance reported by Edwards and Tobin.[2]

Figure 2 presents the results for the apparent emittance of rectangular groove cavities with specularly reflecting metallic walls. Results for the case of dielectric walls can also be obtained in a similar manner. The effect of polarization is illustrated by the comparison in Fig. 2 between the present results and those of Sparrow and Jonsson[4] who neglected polarization in their calculation. It is clearly indicated that the polarization effect is indeed significant in this case.

References

[1] Edwards, D. K. and Bevans, J. T., "Effect of Polarization on Spacecraft Radiation Heat Transfer," *AIAA Journal*, Vol. 3, 1965, p. 1323.

[2] Edwards, D. K. and Tobin, R. D., "Effect of Polarization on Radiant Heat Transfer through Long Passages," *Journal of Heat Transfer*, 89C, 1967, pp. 132–138.

[3] Toor, J. S., Viskanta, R., and Winter, E. R. F., "Effects of Polarization on Radiant Heat Interchange Between Singly Arranged Surfaces," *AIAA Journal*, Vol. 8, No. 5, May 1970, pp. 981–983.

[4] Sparrow, E. M. and Jonsson, V. K., "Thermal Radiation Absorption in Rectangular-Groove Cavities," *Journal of Applied Mechanics*, 85E, 1963, pp. 237–244.

[5] Sparrow, E. M. and Cess, R. D., *Radiation Heat Transfer*, revised edition, Brooks/Cole, Belmont, Calif., 1970.

Effect of Ground Wind Shear on Aircraft Trailing Vortices

DAVID C. BURNHAM*

U. S. Department of Transportation, Cambridge, Mass.

THE motion of the pair of trailing vortices generated by an aircraft is not well described by simple line vortex theory in the presence of a cross wind near the ground. Experimental observations indicate that the up-wind vortex usually drops to a lower altitude than the down-wind vortex. Figure 1 shows a photograph of this phenomenon where the vortex locations are marked by smoke from a tower. Figure 2 shows typical vortex trajectories measured with a pulsed acoustic ranging system developed at this center.

The standard way of calculating the effect of a cross wind on the vortex motion is to add the horizontal wind velocity to the normal[1] induced motion of the vortices. According to this description. the two vortices always remain at equal altitudes. This treatment is inadequate because it neglects the vorticity which is present in the wind shear layer near the ground.

In order to understand the observed asymmetry in vortex height, a self-consistent two-dimensional calculation was made of the vortex motion for a simple model in which all the vorticity

Received February 22, 1972; revision received April 10, 1972.

Index category: Jets, Wakes, and Viscid-Invicid Flow Interactions.

* Staff Scientist, Transportation Systems Center.

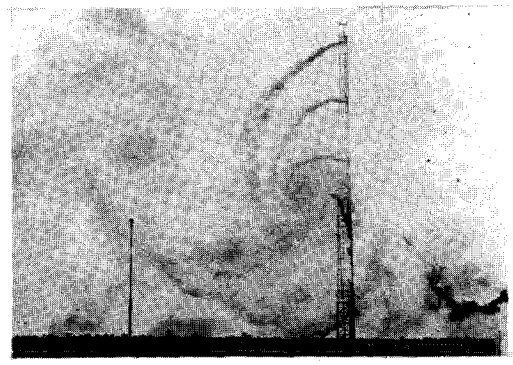

Fig. 1 Photograph of a vortex pair with smoke visualization; note wind direction and upward displacement of vortex on the left. (Courtesy of the Federal Aviation Administration.)

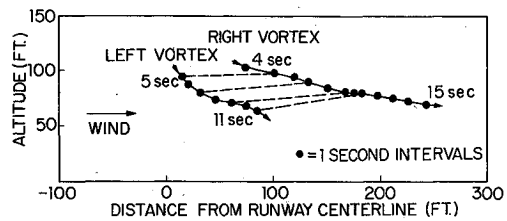

Fig. 2 Trajectories of vortices generated by a B-727 approaching Logan International Airport, runway 22L.

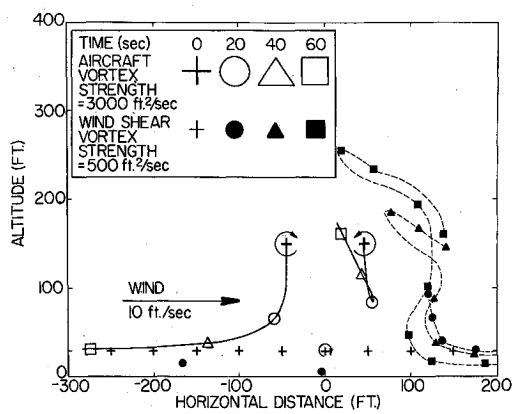

Fig. 3 Calculated vortex trajectories in the frame of reference moving with the wind; 21 wind shear vortices were initially located at 30 ft altitude and 50 ft intervals between −400 and +600 ft.

of the ground shear layer is concentrated into a series of evenly spaced line vortices at a particular altitude. Although this model leads to an unrealistic wind field near each wind shear vortex, it will give a reasonable description of winds at distances larger than the vortex spacing ΔX. In particular, the high altitude (i.e. altitude $\gg \Delta X$) wind is given by the expression $V = \Gamma/\Delta X$ where Γ is the strength (circulation) of each wind shear vortex. In the calculation all vortices above the ground (altitude Y) were paired with oppositely rotating image vortices (altitude ϕY) in order to satisfy the boundary condition of no vertical wind at the ground. The induced motion of each vortex by all the other vortices was then evaluated in order to find the vortex trajectories. The computer time required to carry out this procedure is proportional to $mn(n-1)$ where m is the number of time increments and n is the total number of vortices. Because of this restriction, a rather coarse grid of points was used. The horizontal extent of the wind shear vortices was made large enough that end effects could be ignored without introducing drastic errors in the region near the aircraft vortices.

The results of one such calculation are shown in Fig. 3 where the aircraft vortex parameters are those corresponding to a